PAPER

Check for updates

The influence of elongation-induced concentration fluctuations on segmental friction in polymer blends

Yangyang Wang, [iD] *[a] Shalin Patil,[b] Shiwang Cheng [iD] *[b] and Changwoo Do [iD] [c]

Recent experimental studies have revealed a lack of universality in the extensional behavior of linear polymers, which is not envisioned by classical molecular theories. These surprising findings, particularly the sharp contrast between polymer melts and solutions, have catalyzed the development of new theoretical ideas, including the concept of friction reduction in highly stretched polymer melts. By presenting evidence from rheology and small-angle neutron scattering, this work shows that deformation-induced demixing, which is due to the viscoelastic asymmetry in binary mixtures, contributes to the observed nonuniversality. In the case of polystyrene/oligostyrene blends, demixing increases the effective glass transition temperature of the long chain, leading to an apparent friction enhancement. On the other hand, the opposite case is found for the polystyrene/poly(α-methylstyrene) blend. These results highlight the important influence of deformation-induced concentration fluctuations on polymer segmental friction.

1 Introduction

The dynamic properties of polymeric liquids exhibit remarkable universalities and can often be understood using coarse-grained models.[1–11] In particular, universality has been found in both linear and nonlinear shear rheology of polymer melts and solutions.[2,4,10–20] It is against this backdrop that the observations of lack of universality in the extensional rheology of polymers,[20–33] especially entangled polymers, come as a surprise. Several theoretical ideas, notably interchain pressure[34] and friction reduction,[31,35–41] have been proposed to reconcile these experimental results, but a clear understanding has not been achieved.

The goal of this work is to investigate the potential role of deformation-induced demixing in the apparent lack of universality in extensional rheology of polymers. Although deformation-induced demixing and concentration fluctuations are ubiquitous and well-known phenomena,[42–73] their impact on the rheological behavior of polymers has not been seriously contemplated. As we shall demonstrate below, deformation-induced demixing can not only be present in extensional flow of polymer solutions, but can also affect the rheological response. To illustrate the first point, we

have carried out small-angle neutron scattering measurements of entangled polystyrene solutions during continuous uniaxial extension as well as step-strain relaxation. It is found that the viscoelastic asymmetry between the long and short chains drives the deformation-induced demixing, which occurs on time scales longer than the Rouse relaxation time of the short-chain, oligomeric styrene. Most importantly, demixing leads to a change in the effective glass transition temperature of the long chain. A qualitative theoretical picture is offered to rationalize the anomalous rheological behavior, which exhibits apparent dependence on sample composition (chemistry) and violates the principle of time–temperature equivalence. These results point to the crucial influence of deformation-induced concentration fluctuations on polymer segmental friction.

This paper is organized as follows. The Materials and methods section gives an account of the sample preparation procedures, characterization methods, and equilibrium properties of the polymer solutions. The results of the small-angle neutron scattering experiments are presented and discussed in the first part of the Results and discussion section, and the underlying physics of the deformation-induced demixing is explained. Next, the rheological consequences of demixing are discussed. The change of local glass transition temperature due to the deformation-induced concentration fluctuations turns out to be a key for understanding many aspects of the apparent lack of universality in extensional rheology of polymers, including the molecular weight and temperature effects. Lastly, to put the current investigation into a proper context, we

[a] *Center for Nanophase Materials Sciences, Oak Ridge National Laboratory, Oak Ridge, Tennessee 37831, USA. E-mail: wangy@ornl.gov*

[b] *Department of Chemical Engineering and Materials Science, Michigan State University, East Lansing, MI 48824, USA. E-mail: chengsh9@msu.edu*

[c] *Neutron Scattering Division, Oak Ridge National Laboratory, Oak Ridge, Tennessee 37831, USA*

reexamine the literature data in light of the demixing phenomenon. It is shown that these existing experimental studies indeed should involve deformation-induced demixing, whose influence on the segmental friction should be of vital importance.

2 Materials and methods

2.1 Materials

Hydrogenous (h) and deuterated (d) polystyrenes (PS) with narrow molecular weight distributions were purchased from Polymer Source, Inc. and Scientific Polymer Products Inc., along with a hydrogenous, low molecular weight poly(α-methylstyrene) (PαMS). The molecular characteristics of these samples, including the number average molecular weight (M_n), weight average molecular weight (M_w), and glass transition temperature (T_g), are provided in Table 1. Four binary polymer blends, each consisting of long and short chains, were prepared by dissolving the two components in toluene and subsequently precipitating the polymers in methanol. Due to the lack of a complete set of melt density data for all the samples, the following glassy state densities (ρ_0) were used in the sample preparation and the other calculations: 1.05 g cm^{-3} for h-PS,[74] 1.065 g cm^{-3} for h-PαMS,[74] and 1.12 g cm^{-3} for d-PS.[75] The precipitated polymer blends were dried in a heated vacuum oven above the glass transition temperatures for at least 24 hours to remove any residual solvents. The compositions of these polymer blends are described in Table 2, where Z is the number of entanglements per chain, and ϕ_L and ϕ_S are the volume fractions of the long and short chains, respectively. The PS790K/PS4K, PS790K/PS23K, and PS130K/PS12K blends were used in the small-angle neutron scattering (SANS) experiments, whereas the melt uniaxial extension behavior of PS790K/PS4K, PS790K/PS23K, and PS790K/PαMS11K blends was examined with an SER3 fixture (Xpansion Instruments).[76]

The samples for the SANS experiments were molded into rectangular strips in a Carver hydraulic press at 180 °C. The prepared specimens were uniaxially stretched on a RSA-G2 solid analyzer (TA Instruments) equipped with an environmental test chamber, following well-established procedures.[77–80] In each extension experiment, the polymer sample was stretched with a constant crosshead velocity to a stretching ratio of $\lambda = 1.8$ in the melt state, allowed to relax for a certain amount of time t_{relax}, and then immediately quenched into the glassy state by pumping cold gas into the test chamber. For "continuous" extension experiments, the waiting time (i.e., stress relaxation

time) $t_{relax} = 0$. The initial strain rate $\dot{\varepsilon}_0$ is given by the crosshead velocity v_0 and initial length of the sample l_0 as $\dot{\varepsilon}_0 = v_0/l_0$. Additionally, the quenching time was always significantly shorter than the waiting time as well as the Rouse relaxation time of the sample. This kind of stretch–quench method thus effectively preserved the "instantaneous" polymer structures for the ex situ SANS characterization.

Because of the constraint of test chamber size, the stretching experiments on RSA-G2 were limited to moderate strains. Therefore, a more complete set of melt extension data was collected with a SER3 fixture fitted on an MCR302 rheometer (Anton Paar). The temperature control was achieved using a CTD600 environmental chamber, with an accuracy of ±0.1 °C. The samples were prepared in the form of filaments (1 mm in diameter) by melt extrusion with a Monsanto capillary rheometer at $T = 160$ °C.[81] Continuous uniaxial extension experiments were carried out under constant Hencky strain rates $\dot{\varepsilon}$ with nitrogen as the gas source.

2.2 Differential scanning calorimetry

Differential scanning calorimetry (DSC) measurements of the neat polymers as well as the polymer blends were carried out on a DSC Q2000 from TA Instruments with aluminum hermetic pans. The glass transition temperature (T_g) was determined from the heat flow during the heating scan using the "half extrapolated tangents" method. For each sample, three heating scans were performed with rates 10 °C min^{-1}, 5 °C min^{-1}, and 2 °C min^{-1}, respectively, and the glass transition temperatures reported in Table 1 are based on linear extrapolations to zero heating rate. To further illustrate the influence of molecular weight on the glass transition temperature, the data of all the polystyrene samples are also plotted in the inset of Fig. 1.

The low-molecular-weight PS4K has the lowest T_g among all the samples, around 80 °C. On the other hand, the T_g of PS23K is only slightly lower than that of PS790K. In these polystyrene–polystyrene (oligostyrene) blends, the T_g of the short chain (solvent) is always lower than that of the long chain. In contrast, in the PS790K/PαMS11K blend, the short PαMS11K has higher T_g (156.1 ± 1.2 °C) than the long chain ($T_g = 104.0 ± 0.9$ °C). As we shall see later, this kind of "reversed" blend provides important insight into the influence of deformation-induced demixing on rheology.

2.3 Rheology

Small-amplitude oscillatory shear measurements were carried out on an HR2 (TA Instruments) rheometer with parallel plates to evaluate the linear viscoelastic properties of the polystyrene samples. The time–temperature superposition (TTS) principle[4]

Table 2 Compositions of the polymer blends

Blend name	Long chain	Short chain	ϕ_L	ϕ_S	Z
PS790K/PS4K	h-PS790K	d-PS4K	0.56	0.44	21
PS790K/PS23K	h-PS790K	d-PS23K	0.56	0.44	24
PS130K/PS12K	d-PS130K	h-PS12K	0.50	0.50	2.7
PS790K/PαMS11K	h-PS790K	h-PαMS11K	0.56	0.44	26

Table 1 Molecular characteristics of the samples used in this work

Sample name	M_n (kg mol^{-1})	M_w (kg mol^{-1})	M_w/M_n	T_g [°C]
h-PS790K	790	853	1.08	104.0 ± 0.9
d-PS23K	23.0	24.4	1.06	100.3 ± 1.4
d-PS4K	4.00	4.30	1.07	80.0 ± 0.8
d-PS130K	125	133	1.06	101.8 ± 1.4
h-PS12K	12.0	12.1	1.01	89.4 ± 0.4
h-PαMS11K	10.6	11.8	1.11	156.1 ± 1.2

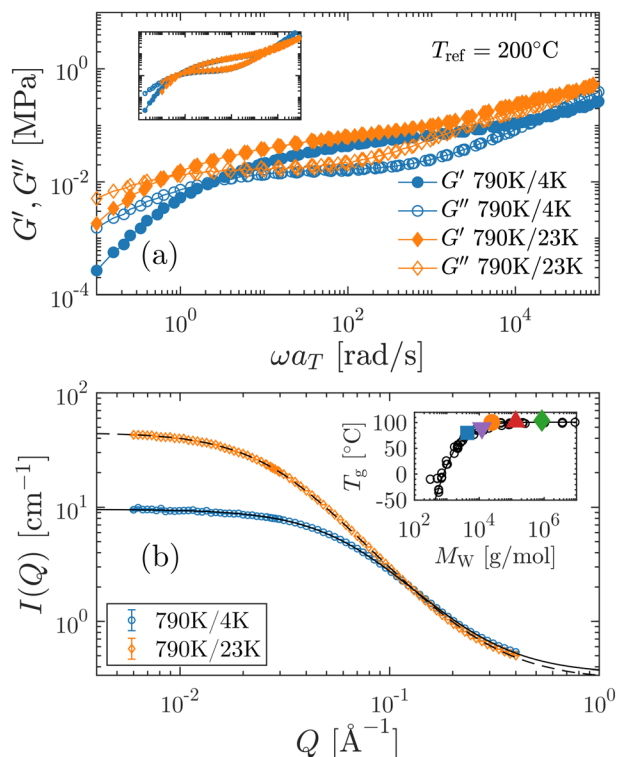**Fig. 1** (a) Linear viscoelastic spectra of the PS790K/PS4K and PS790K/PS23K blends at T = 200 °C. The inset shows that the dynamic moduli of the two samples can be overlapped with appropriate horizontal shifts. (b) SANS spectra of the polymer blends in the isotropic, undeformed state. Symbols: experimental data. Lines: Fittings with the RPA equation. The inset presents the glass transition temperature T_gs of PS4K (square), PS12K (down triangle), PS23K (circle), PS130K (up triangle), and PS790K (diamond). The black hollow circles are the T_g data from the literature.[82,83]

is used to construct master curves of the measured dynamic moduli ($G^* = G' + iG''$). The linear viscoelastic spectra of PS790K/PS4K and PS790K/23K blends are shown in Fig. 1. These two samples have similar entanglement plateau moduli and widths, and their linear viscoelastic spectra can be overlapped with appropriate shifts in angular frequency [inset of Fig. 1(a)]. Additional results for the PS790K/PS4K, PS790K/PS23K, PS130K/PS12K, and PS790K/PαMS11K blends, as well as those for the neat PS4K, PS23K, PS12K, and PαMS11K melts, are included in Appendix A. The rubbery plateau modulus G_N is determined from the storage modulus $G'(\omega)$ at the frequency where $\tan\delta = G''/G'$ exhibits a minimum. The average number of entanglements per chain $Z = M_w/M_e$ is estimated from the weight-average molecular weight M_w and entanglement molecular weight M_e, with $M_e = \rho_0\phi_L RT/G_N$.[4] Here, ρ_0 and ϕ_L are respectively the density and volume fraction of the long chain, R is the gas constant, and T is the absolute temperature.

For the entangled polymer blends, the terminal relaxation time τ of the long chain is determined from the low-frequency crossover of the storage and loss moduli as $\tau = \omega_c^{-1}$, where ω_c is the crossover angular frequency. For the neat, unentangled polymers (PS4K, PS12K, PS23K, and PαMS11K), the terminal relaxation time is calculated from the steady-state creep

compliance J_e^0 and zero-shear viscosity η_0 as: $\tau = J_e^0\eta_0$.[4] The J_e^0 and η_0 are obtained by fitting the low-frequency dynamic mechanical spectrum:[4]

$$\lim_{\omega\to 0} G'(\omega) = J_e^0\eta_0^2\omega^2,$$
$$\lim_{\omega\to 0} G''(\omega) = \eta_0\omega. \tag{1}$$

The terminal relaxation time of the short chain in the polymer blend can be estimated by using the Lodge–McLeish model.[84,85] The details of component dynamics calculations are provided in Appendix B. The purpose of calculating the relaxation time of the short chains is to demonstrate the time scale of the deformation or stress relaxation relative to the characteristic molecular time scale of the short chains, as deformation-induced demixing occurs only when the short chains have sufficient time to relax and to diffuse over a large distance.[72] For this qualitative analysis, one only needs to arrive at the correct order of magnitude for the relaxation times of the short chains. Please note that the effective applied rate (Wi₀) is determined according to the viscoelastic time of the long chains, which is a well-defined quantity ($\tau = 1/\omega_c$). Different calculation methods may yield slightly different values of relaxation time for the short chains in the blends. However, such discrepancies have no impact on our experiments or discussions.

2.4 Small-angle neutron scattering

Small-angle neutron scattering experiments were performed on the EQ-SANS beamline of the Oak Ridge National Laboratory's Spallation Neutron Source.[86,87] For the PS790K/PS4K and PS790K/PS23K blends, two configurations were used to cover a scattering wavenumber (Q) range of 0.006–0.4 Å⁻¹. The sample to detector distance was fixed at 4 m and two wavelength bands defined by the minimum wavelength of 10 Å and 2.5 Å were used. For the PS130K/PS12K blend, three configurations were used with a Q coverage of 0.003–0.5 Å⁻¹. Here, the sample to detector distance was varied to 2.5 m, 4 m, and 9 m with wavelength bands defined by minimum wavelengths of 2.5 Å, 10 Å, and 15 Å, respectively. The obtained scattering intensities were normalized by the sample thickness, corrected by the detector sensitivity and background contributions, and placed on an absolute scale using measurements of a standard sample.[88,89]

The results of SANS measurements of the isotropic, undeformed polymer blends PS790K/PS4K and PS790K/PS23K are shown in Fig. 1(b). These SANS spectra can be fitted with the widely used random-phase-approximation (RPA) formula:[90,91]

$$\frac{I_{iso}(0) - I_{inc}}{I(Q) - I_{inc}} = \left(\frac{1}{\phi_a N_a \tilde{P}_a(Q)} + \frac{1}{\phi_b N_b \tilde{P}_b(Q)} - 2\chi\right)$$
$$\times \left(\frac{1}{\phi_a N_a} + \frac{1}{\phi_b N_b} - 2\chi\right)^{-1}, \tag{2}$$

where $I(Q)$ is the measured absolute scattering intensity, $I_{iso}(0)$ is the zero-angle scattering intensity, I_{inc} is the incoherent background, χ is the Flory–Huggins interaction parameter,

and ϕ_α, N_α, and $\tilde{P}_\alpha(Q)$ are respectively the volume fraction, degree of polymerization, and single-chain structure factor of component α ($\alpha = a, b$). In the current context, component a is the long chain (L), and b is the short chain (S). With the Gaussian-chain assumption, the single-chain structure factor $\tilde{P}_\alpha(Q)$ takes the form of a Debye function:

$$\tilde{P}_\alpha(Q) = \frac{2}{Q^4 R_{g0,\alpha}{}^4}\left[\exp\left(-Q^2 R_{g0,\alpha}{}^2\right) + Q^2 R_{g0,\alpha}{}^2 - 1\right], \quad (3)$$

where $R_{g0,\alpha}$ is the equilibrium radius of gyration of component α. The volume fractions in eqn (2) are determined by the compositions of the samples and therefore not fitting parameters. The degree of polymerization N_α for each component is calculated according to the weight average molecular weight given by the gel permeation chromatography. The equilibrium radius of gyration $R_{g0,\alpha}$ is estimated according to the formula $\log_{10} R_{g0,\alpha} = 0.4175 + 0.5076 \times \log_{10} N_\alpha$, which is obtained by a linear fit of the literature data.[77-79,92] The resulting fitting curves from eqn (2) are presented in Fig. 1(b). The corresponding fitting parameters are: $I_{iso}(0) = 9.23\,cm^{-1}$, $I_{inc} = 0.34\,cm^{-1}$, and $\chi = 5.6 \times 10^{-3}$ for the 790K/4K blend; $I_{iso}(0) = 44.30\,cm^{-1}$, $I_{inc} = 0.32\,cm^{-1}$, and $\chi = 5.4 \times 10^{-4}$ for the 790K/23K blend. The SANS spectrum of the isotropic, undeformed PS130K/PS12K blend (not shown here) is fitted by the same

procedure, and the result is: $I_{iso}(0) = 23.19\,cm^{-1}$, $I_{inc} = 0.26\,cm^{-1}$, and $\chi \approx 0$. The success of the RPA formula and the relatively low values of χ indicate that the short and long chains are well mixed in the equilibrium, undeformed state. Although we do not have SANS data for the PS790K/PαMS11K blend, our DSC measurement and the previous studies in the literature[93-96] suggest that this particular pair of PS and PαMS should be miscible at $\phi_L = 0.56$.

3 Results and discussion

3.1 Evidence of demixing during continuous extension

The results of SANS measurements of the PS blends during continuous uniaxial extension at various initial Weissenberg numbers ($Wi_0 \equiv \dot{\varepsilon}_0\tau$, defined with respect to the long chain here) are shown in Fig. 2(a) and (b). As noted in the experimental section, all the spectra were taken at a stretching ratio of 1.8. With the exception of the PS790K/PS23K blend at 120 °C and $Wi_0 = 100$ and $Wi_0 = 1000$, butterfly patterns can be observed in all cases. Additionally, the time–temperature superposition principle does not hold in the nonlinear viscoelastic regime, as the scattering pattern is dependent on not only the effective strain rate Wi_0, but also the temperature.
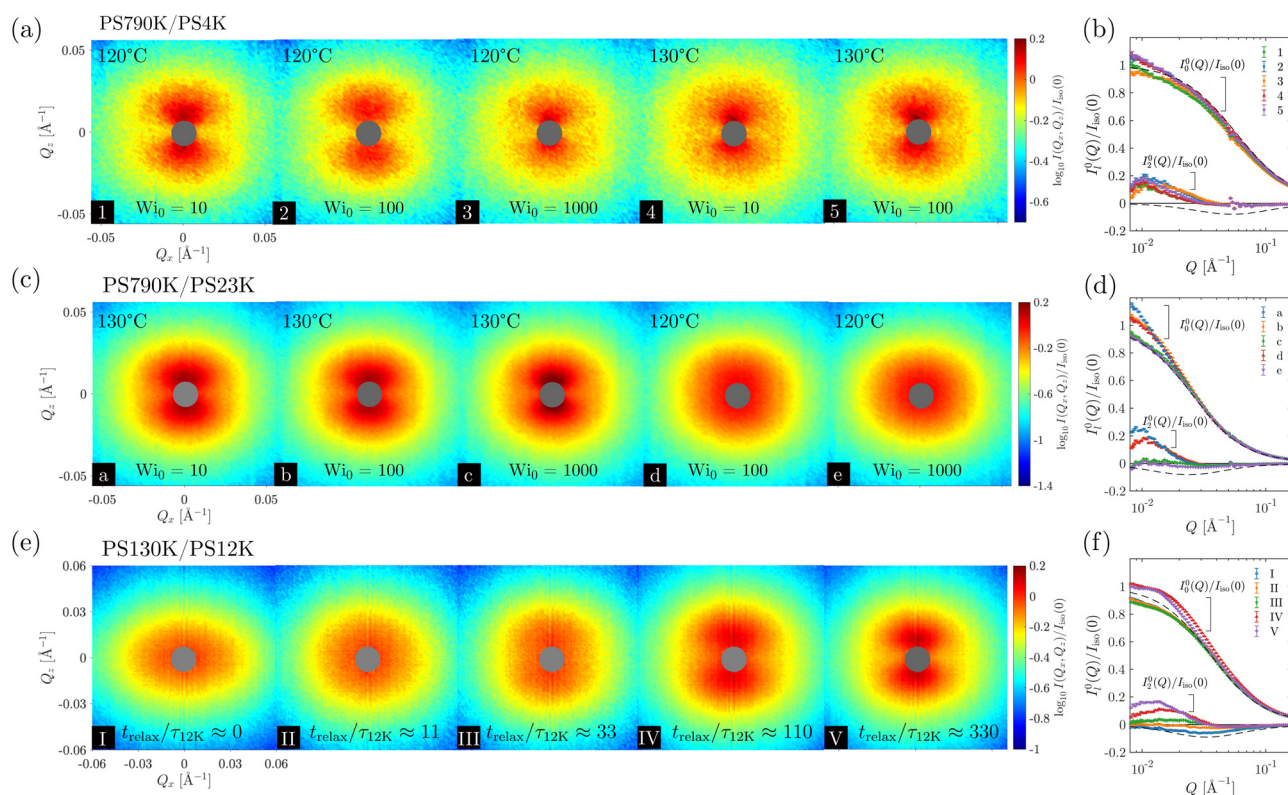

Fig. 2 Results of SANS measurements of deformed polymer blends. (a) SANS spectra of the PS790K/PS4K blend at $\lambda = 1.8$, stretched under different temperatures and initial Weissenberg numbers, Wi_0. (b) Corresponding normalized spherical harmonic expansion coefficients. Here, $I_{iso}(0)$ is the zero-angle scattering intensity of the isotropic, undeformed sample. (c) and (d) The results of the PS790K/PS23K blend at $\lambda = 1.8$. (e) SANS spectra of the PS130K/PS12K blend during stress relaxation, following a step strain of $\lambda = 1.8$. The elapsed time during stress relaxation (t_{relax}) is normalized by the terminal relaxation time of PS12K (τ_{12K}) and displayed at the bottom of each spectrum. (f) The corresponding normalized spherical harmonic expansion coefficients. Dashed lines in the insets: predictions of the RPA model, with the assumption that the long chains obey affine deformation ($\lambda_a = 1.8$) and the short chains are fully relaxed ($\lambda_b = 1$).

To quantify the structural changes under uniaxial extension and better illustrate the failure of TTS, the measured 2D SANS spectra are analyzed with the spherical harmonic expansion technique.[72,77,79,97] Specifically, the scattering intensity $I(\mathbf{Q})$ is expanded as $I(\mathbf{Q}) = \sum_{l:\text{even}} I_l^0(Q) Y_l^0(\theta, \phi)$, where θ is the polar angle, ϕ is the azimuthal angle, $Y_l^0(\theta,\phi)$ is the spherical harmonic function of degree l and order zero, and $I_l^0(Q)$ is the corresponding coefficient. The definitions of the spherical harmonic functions follow the ones used in our previous work,[77] where the normalization condition is $\int Y_l^m(\Omega) Y_{l'}^{m'}(\Omega) \, d\Omega = 4\pi \delta_{l,l'} \delta_{m,m'}$, with $\delta_{l,l'}$ and $\delta_{m,m'}$ being the Kronecker δ-functions. In the case of uniaxial extension, the spherical coordinates are placed in such a way that the z axis is along the stretching direction, and the xz plane is perpendicular to the incident beam and parallel to the sample.[77] The expansion coefficient $I_l^0(Q)$ is related to the experimentally measured scattering intensity from the xz plane $I_{xz}(Q,\theta)$ as:

$$I_l^0(Q) = \frac{1}{2} \int_0^\pi I_{xz}(Q, \theta) \, Y_l^0(\theta) \sin\theta \, d\theta. \tag{4}$$

In other words, the spherical harmonic expansion coefficients can be obtained from weighted integrals of the 2D SANS spectrum with Legendre functions. Generally speaking, the isotropic expansion coefficient $I_0^0(Q)$ and leading anisotropic expansion coefficient $I_2^0(Q)$ are the most important ones,[72] and they are shown in Fig. 2(b) and (d) for the SANS spectra from continuous uniaxial extension. To appropriately compare different samples, these coefficients are normalized by the zero-angle scattering intensity of the isotropic, undeformed sample $I_{\text{iso}}(0)$. As discussed in our previous studies,[72,77,79] the sign of the leading anisotropic expansion coefficient $I_2^0(Q)$ is connected to the symmetry of the underlying molecular correlations: for stretched polymers, a negative $I_2^0(Q)$ is a result of the growing intrachain correlations of the elongated molecule of along the stretching direction; a positive $I_2^0(Q)$ is often associated with the long-range interchain correlations in the perpendicular direction due to short chain migration. On the other hand, the magnitude of $I_0^0(Q)$ in the zero-angle limit can reflect the degree of mixing—a phase separated system would exhibit enhanced zero-angle scattering.

To further enhance insight, we compute the spherical harmonic expansion coefficients of the blends using the random-phase approximation, where the mixing state is assumed to be unaffected by the deformation. The normalized anisotropic scattering intensity $I(\mathbf{Q})/I_{\text{iso}}(0)$ is given by

$$\frac{I(\mathbf{Q})}{I_{\text{iso}}(0)} = \left(\frac{I_{\text{iso}}(0) - I_{\text{inc}}}{I_{\text{iso}}(0)} \right) \left(\frac{1}{\phi_a N_a \tilde{P}_a(\mathbf{Q})} + \frac{1}{\phi_b N_b \tilde{P}_b(\mathbf{Q})} - 2\chi \right)^{-1}$$
$$\times \left(\frac{1}{\phi_a N_a} + \frac{1}{\phi_b N_b} - 2\chi \right) + \frac{I_{\text{inc}}}{I_{\text{iso}}(0)}, \tag{5}$$

where

$$\tilde{P}_\alpha(\mathbf{Q}) = \tilde{P}_\alpha(Q_x, Q_y, Q_z) = \frac{2}{x^2}(\exp(-x) + x - 1), \tag{6}$$

with

$$x = R_{g0,\alpha}^2 (\lambda_\alpha^{-1} Q_x^2 + \lambda_\alpha^{-1} Q_y^2 + \lambda_\alpha^2 Q_z^2). \tag{7}$$

Under the current experimental condition, $\text{Wi}_0 \gg 1$ for the long chains in the blends and $\text{Wi}_0 \ll 1$ for the short-chain solvents. Therefore, we make the simple assumption that the long chains obey affine deformation ($\lambda_a = 1.8$), whereas the short chains are fully relaxed ($\lambda_b = 1$). The rest of the parameters in eqn (5) can be obtained from the fittings of the isotropic samples. The normalized spherical harmonic expansion coefficients from the RPA model can be straightforwardly computed as

$$\frac{I_l^0(Q)}{I_{\text{iso}}(0)} = \frac{1}{4\pi} \int_0^{2\pi} d\phi \int_0^\pi \sin\theta \, d\theta \frac{I(\mathbf{Q})}{I_{\text{iso}}(0)} Y_l^0(\theta, \phi). \tag{8}$$

The results of RPA calculations are presented in Fig. 2 as reference curves. As pointed out previously, the RPA model by definition cannot handle deformation-induced demixing and is incapable of producing butterfly patterns.[72]

Several observations from the spherical harmonic expansion analysis are worth noting. First, our previous study demonstrated that positive $I_2^0(Q)$ is associated with butterfly scattering patterns whereas negative $I_2^0(Q)$ produces ellipsoidal patterns.[72] The current results in Fig. 2 are consistent with this prior finding: the anisotropic expansion coefficients $I_2^0(Q)$ are positive within the experimental Q range for the butterfly patterns (spectra 1–5, a, b, and c); the $I_2^0(Q)$ is close to zero for the SANS spectrum of the PS790K/PS23K blend at $\text{Wi}_0 = 100$ and 120 °C (spectrum d); and the $I_2^0(Q)$ is slightly negative for the ellipsoidal spectrum of PS790K/PS23K at $\text{Wi}_0 = 1000$ and 120 °C (spectrum e). Second, the failure of TTS becomes quite evident, when the 2D SANS spectra are quantified by the spherical harmonic expansion technique. The expansion coefficients $I_0^0(Q)$ and $I_2^0(Q)$ are not identical for the same sample stretched under the same Wi_0. Third, the short-chain molecular weight clearly plays a role in the structural evolution during extension, even when Wi_0 and temperature are kept the same (e.g., spectra 3 and e). This behavior is consistent with the previous reports of a lack of universality in the uniaxial extension of entangled polymers,[26,33] where the solvent molecular weight effect was observed. Lastly, a comparison with the RPA reference curves (dashed lines) suggests that some degree of deformation-induced demixing is still present in the samples that do not exhibit butterfly patterns [spectra (d) and (e)], as their anisotropic coefficients $I_2^0(Q)$ are substantially smaller than the RPA predictions (in magnitude). This is due to the cancellation effect from intramolecular and intermolecular correlations.[72]

The emergence of butterfly patterns is a direct result of deformation-induced demixing,[72] which has been attributed to the asymmetric stress division in polymer blends that drives diffusion of short chains in the direction perpendicular to stretching.[98–102] Our previous investigation[72] indicates that $\text{Wi}_0 \ll 1$ for the short chain is a necessary condition for generating butterfly patterns, i.e., deformation-induced demixing in polymer blends. Using the Lodge–McLeish model, the short-chain relaxation time in the blend can be estimated (see Appendix B for details). Combined with the long-chain relaxation time

directly measured by small-amplitude oscillatory shear, we find that the ratio of long chain and short chain terminal relaxation times is approximately 3.3×10^5 for the PS790K/PS4K at the experimental temperatures, and 1.0×10^4 for the PS790K/PS23K. The condition of $Wi_0 \ll 1$ is thus satisfied for both PS4K and PS23K in these blends. Nevertheless, the difference in the glass transition temperature and relaxation time of the short chains should play an important role in the lack of universality in the extensional rheology of these polymer blends. The full consequence of deformation-induced demixing on the rheological behavior will be discussed in detail in Section 3.3. It is worth noting that the deformation-induced demixing is directly connected to the diffusive kinetics of the short chains and the enhanced concentration fluctuations at lower Wi_0 [Fig. 2(a)–(d) are a result of the prolonged time for molecular diffusion.[72]

3.2 Evidence of demixing during stress relaxation

To illustrate the ubiquity of the deformation-induced demixing in polymer blends, we now turn our attention to stress relaxation. In this case, the PS130K/PS12K blend was uniaxially stretched to an extension ratio of $\lambda = 1.8$ at 110 °C with an effective initial Weissenberg number $Wi_0 = 1.9 \times 10^2$ for the long chain ($Wi_0 \ll 1$ for the short chain), allowed to relax for $t_{relax} = 0$, 100, 300, 1000, and 3000 s, and subsequently quenched into the glassy state for *ex situ* SANS measurements. The terminal relaxation times τ of the long and short chains are about 1.9×10^4 and 9 s respectively at the experimental temperature of 110 °C. Therefore, even at the longest time of $t_{relax} = 3000$ s, the long chains still retain a substantial amount of stress whereas the short chains have sufficient time to relax and diffuse over a large distance. The results of the SANS experiments are shown in Fig. 2(e) and (f), and the corresponding stress data are presented in Fig. 3.

Immediately after the step deformation ($t_{relax} \approx 0$), the SANS spectrum displays an ellipsoidal pattern, suggesting that the coherent scattering is dominated by the intramolecular correlations of the stretched chain [spectrum I of Fig. 2(e)]. Nevertheless, a weak degree of demixing may have occurred during the step extension, as the duration of the deformation is longer than the relaxation time of the short chain. Quantitative analysis with the spherical harmonic expansion technique seems to confirm this conclusion [Fig. 2(f)], as the experimental structural anisotropy $I_2^0(Q)$ is still smaller than the RPA prediction. With the progression of stress relaxation, the short chains continue to migrate in the direction perpendicular to stretching, due to the viscoelastic asymmetry between long and short chains. Consequently, butterfly patterns start to develop. This process is clearly captured by the spherical harmonic expansion analysis—demixing leads to a change of sign in $I_2^0(Q)$ and an enhancement of the isotropic, zero-angle scattering intensity.[72]

The stress relaxation experiment is a powerful demonstration of the nature of deformation-induced demixing—it is not caused by convection itself, but the viscoelastic asymmetry of the two components, *i.e.*, the coexistence of fast- and slow-relaxing chains.[98–101] Since the underlying physics here is entirely general, deformation-induced demixing should be present in many polymer
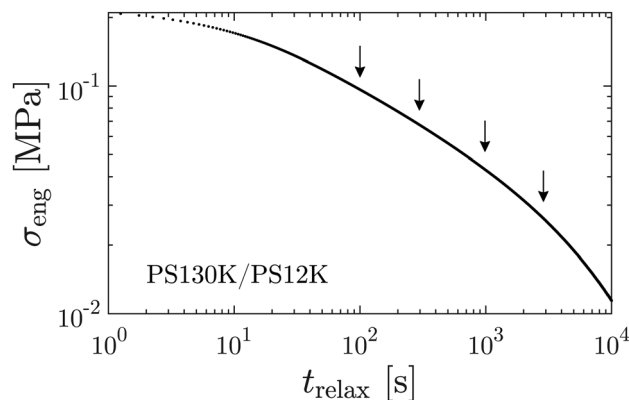

Fig. 3 Stress relaxation behavior of the PS130K/PS12K blend after a step uniaxial extension of $\lambda = 1.8$. σ_{eng} is the engineering stress defined by the tensile force and the initial cross-sectional area of the sample. The arrows indicate the relaxation states (*i.e.*, $t_{relax} = 100$, 300, 1000, and 3000 s or equivalently 11, 33, 110, and $330\tau_{12K}$) that are examined by small-angle neutron scattering.

blends and solutions—a fact that is often underappreciated in rheological measurements at large deformations. In the next section, we will explore the consequence of deformation-induced demixing and explain its important role in the loss of universality in extensional rheology of entangled polymers.

In passing, we note that a previous SANS investigation of PS blends during stress relaxation did not reveal any butterfly patterns.[103] A closer look at their experimental conditions indicates, however, that the SANS spectra were taken up to only two times of the relaxation time of the short chain, which would be insufficient for full development of deformation-induced demixing. In other words, there is no contradiction between the current and previous reports.

3.3 Consequence of demixing: change of local friction

Now we ask the most important question: what is the consequence of deformation-induced demixing and how is it related to the lack of universality in extensional rheology of polymers? We observe that in many polymer blends and solutions, the short chains or solvent molecules have a much lower glass transition temperature than the long chains. As the long chain and solvent demix under deformation, the effective glass transition temperature of the long chain, which controls the rheological response, should start to increase. In other words, deformation-induced demixing leads to an increase of the local friction of the long chain in such blends or solutions. This picture offers an important clue for understanding the sharp contrast between polymer melts and solutions in steady extensional flow, where melts display thinning behavior and solutions exhibit hardening behavior.[24] Since the "standard" tube model predicts a hardening behavior of steady-state extensional viscosity of entangled polymers when the Rouse Weissenberg number is greater than unity,[34] which is in apparent, qualitative agreement with the experimental data on polymer solutions but at odds with the data on polymer melts, recent research attention has been focused on searching for a friction reduction mechanism in polymer melts to explain its extensional thinning behavior.

We argue that the effect of deformation-induced demixing is also of great importance in understanding the differences in the rheological behaviors among polymer blends, solutions, and melts, where the presence of viscoelastic asymmetry is almost ubiquitous in the former two.[69,104,105]

To further test the proposed picture, we now take a closer look at the rheological behavior of deformed polymer blends. In the present analysis, we will highlight two noteworthy consequences of deformation-induced demixing. One concerns the effect of short-chain molecular weight on the rheological behavior of polymer blends, and the other relates to the failure of time–temperature superposition (TTS) in the large-deformation limit. Both of them derive from the change in local friction associated with demixing.

3.3.1 Molecular weight effect. An important consequence of the demixing-induced change of local friction is that it offers a natural explanation, at least partially, to the observed molecular weight effect in extensional rheology of entangled polymers.[26] It was observed previously that polymer solutions (blends) with lower molecular weight macromolecular "solvent" produce a higher degree of strain hardening in steady extensional flow.[26] Since the glass transition temperature of polystyrene is strongly dependent on the molecular weight below *ca.* 30 kg mol^{-1}, the lower molecular weight solvent should produce a larger increase of the effective T_g for the long chain upon demixing. At the same Weissenberg/Rouse Weissenberg number as determined from the equilibrium state, the effective rate would be much higher for the solution with short chains of lower molecular weight.

The above explanation is not only consistent with the steady-state data in the literature[26] but is also supported by the transient stress–strain data from the current investigation. Fig. 4(a) compares the stress–strain behavior of PS790K/PS4K and PS790K/PS23K at Weissenberg numbers (Wi $\equiv \dot{\varepsilon}\tau$) of 63 and 1000 at 140 °C. Here, the Weissenberg number is computed using the terminal relaxation time of the long chain (blend) in the equilibrium, mixed state. The DSC measurements (Table 1) indicate that the d-PS4K has a glass transition temperature around 80 °C, whereas the d-PS23K has a T_g around 100 °C, which is fairly close to that of the h-PS790K (104 °C). Therefore, deformation-induced demixing should have a much larger impact on the effective T_g of PS790K in PS790K/PS4K than in PS790K/PS23K. In accordance with our expectation, the PS790K/PS4K exhibits higher stress than the PS790K/PS23K at large strains. Therefore, a proper understanding of such phenomena should require consideration of the change in local effective glass transition temperature due to demixing, besides the potential influence of nematic interactions.[26,106–109]

3.3.2 Temperature effect. Another crucial consequence of the demixing-induced change of local friction concerns the breakdown of time–temperature superposition in nonlinear extensional deformation of polymer blends and solutions.[33] The failure of TTS in miscible polymer blends with large dynamic asymmetry in the equilibrium state is a well-known phenomenon,[110] although it does not occur in every system. In fact, TTS typically works reasonably well for slow linear
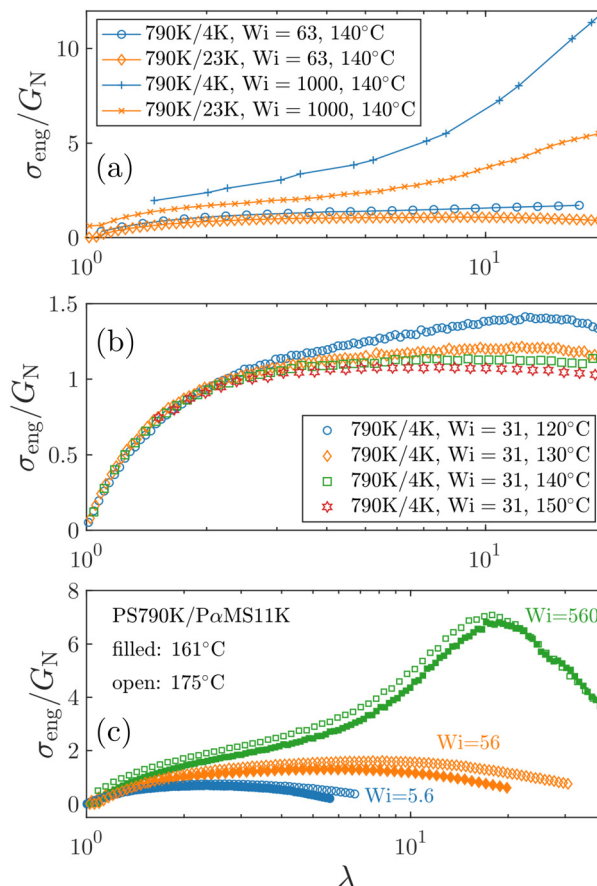

Fig. 4 Normalized engineering stress σ_{eng}/G_N as a function of the stretching ratio λ. (a) Comparison of PS790K/PS4K and PS790K/PS23K at the same Weissenberg number (Wi). (b) Temperature dependence of the stress–strain behavior of PS790K/PS4K at the same Wi. (c) Temperature dependence of the stress–strain behavior of PS790K/PαMS11K at the same Wi.

viscoelastic responses of polymer blends and solutions,[111,112] where the characteristic terminal relaxation times of long and short chains are widely separated. This is also the case for the linear dynamic mechanical spectra of the present polymer blends, as determined by the small-amplitude oscillatory shear measurements (Fig. 1 and 6). However, the time–temperature superposition principle can break down in polymer blends at large deformation.[33]

An example of such a breakdown is illustrated in Fig. 4(b). As described in the Materials and methods section, constant Hencky-strain-rate extension experiments were carried out on the PS790K/PS4K blend up to a stretching ratio of at least $\lambda = 20$. Fig. 4(b) compares the stress–strain curves produced with the same Weissenberg number Wi = 31 at 120 °C, 130 °C, 140 °C, and 150 °C. The linear and quasi-linear responses at relatively small strains are essentially identical at different temperatures, which is in agreement with the time–temperature superposition principle. However, clear differences are observed at large strains, as the stress level increases with the decrease of temperature—this is an apparent violation of the TTS principle. Similar trends have been found for both PS790K/PS4K and PS790K/PS23K at other Weissenberg numbers.

This seemingly perplexing phenomenon can be qualitatively understood in terms of the demixing-induced change of local friction. In the current case of mixtures of high-T_g long chains and low-T_g short chains, the stress response is dominated by the long chains, which acquire a higher effective glass transition temperature $\hat{T}_{g,L}^{eff}$ upon deformation-induced demixing. Here, the hat symbol denotes properties associated with the demixed states. Fig. 5 schematically illustrates the temperature dependence of the local friction of the long chain in both the equilibrium ($\zeta_L(T)$, solid line) and demixed states ($\hat{\zeta}_L(T)$, dashed line). It is easy to see that for two temperatures T_1 and T_2 ($T_1 < T_2$), the following relationship should be true for the local frictions in the equilibrium and nonequilibrium states:

$$\frac{\hat{\zeta}_L(T_1)}{\hat{\zeta}_L(T_2)} > \frac{\zeta_L(T_1)}{\zeta_L(T_2)}. \tag{9}$$

In other words, the friction of the long chain in the demixed state should be more sensitive to the change of temperature, because of its elevated effective glass transition temperature. For extension experiments at the same Weissenberg number at T_1 and T_2, the applied strain rates are selected according to the friction coefficients at the equilibrium state: $\zeta_L(T_1)\dot{\varepsilon}(T_1) = \zeta_L(T_2)\dot{\varepsilon}(T_2)$. Therefore, following the inequality in eqn (9), the effective rate in the demixed state at the low temperature T_1 must be higher than that at the high temperature T_2: $\hat{\zeta}_L(T_1)\dot{\varepsilon}(T_1) > \hat{\zeta}_L(T_2)\dot{\varepsilon}(T_2)$. This partially explains the observed failure of TTS—it breaks down as a result of a change in local friction associated with deformation-induced demixing.

To provide further support to the preceding argument, we turn to the PS790K/PαMS11K blend. In this system, the short PαMS11K chain has a higher T_g than the long PS790K chain, while the terminal relaxation times of the short and long chains

remain widely separated in the blend (Fig. 6 and 7). Therefore, the viscoelastic asymmetry should still drive demixing under deformation, but the long chain should experience a decrease in effective T_g and thus a reduction of local friction in the nonequilibrium state—exactly the opposite case of the PS/PS blend. For extension experiments at the same Weissenberg number at T_1 and T_2 ($T_1 < T_2$), the effective rate should now be lower at the low temperature T_1: $\hat{\zeta}_L(T_1)\dot{\varepsilon}(T_1) < \hat{\zeta}_L(T_2)\dot{\varepsilon}(T_2)$ (Fig. 5). This prediction is indeed verified experimentally in the PS790K/PαMS11K blend, as shown in Fig. 4(c).

We note that our argument about the dependence of the temperature sensitivity of ζ_L on T_g [e.g. eqn (9)] can be placed on a firm mathematical basis with the aid of the Williams–Landel–Ferry (WLF) equation,[4] by assuming that the change of local composition alters the reference temperature but not the coefficients C_1 and C_2. This is in fact a common assumption in the context of the concentration fluctuation effect on segmental dynamics in miscible polymer blends.[85,113]

3.4 Ubiquity of demixing: a literature survey

Lastly, it is important to recognize that deformation-induced demixing is present in many polymer blends and solutions of practical interest. For example, the recent discussions of non-universal extensional rheology of polymers polystyrene/oligostyrene blends,[26,27,29,30] poly(methyl methacrylate)/oligo(methyl methacrylate) blends,[32,114] and polymer solutions with marginal solvent quality, including PS/diethyl phthalate (DEP),[21,22,28] PS/dibutyl phthalate (DBP),[21,22,27] PS/dioctyl phthalate (DOP),[21] PS/tricresyl phosphate (TCP),[23] and polyisoprene/squalene.[28]
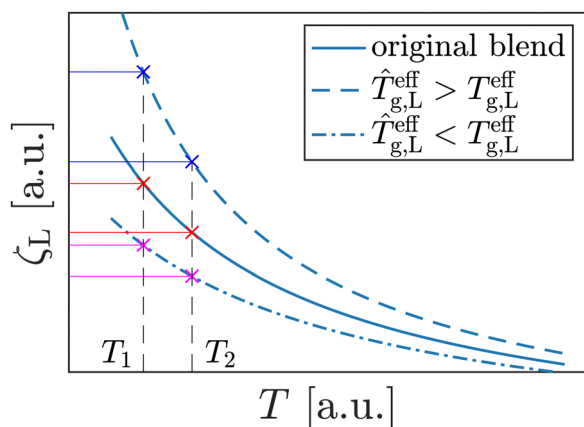

Fig. 5 Illustration of the change of local friction ζ_L for the long chain in deformed polymer blends. Solid line: original blend in the equilibrium state. The dashed line depicts the long chain friction $\hat{\zeta}_L$ in the nonequilibrium state, where demixing leads to an increase in effective glass transition temperature $\hat{T}_{g,L}^{eff}$ for the long chain ($\hat{T}_{g,L}^{eff} > T_{g,L}^{eff}$). The dash-dotted line represents the opposite case, where the effective glass transition temperature decreases upon demixing ($\hat{T}_{g,L}^{eff} < T_{g,L}^{eff}$). Here, $T_{g,L}^{eff}$ and $\hat{T}_{g,L}^{eff}$ are the effective glass transition temperatures of the long chain in equilibrium and demixed states, respectively. The horizontal solid lines help to visualize the change in the ratio of friction coefficients at T_1 and T_2 in different states.
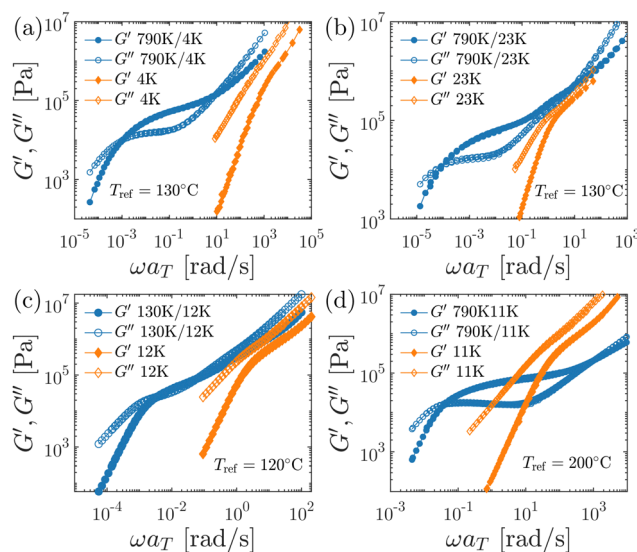

Fig. 6 Linear viscoelastic spectra of PS790K/PS4K and PS790K/PS23K PS blends, as well as the corresponding polystyrene "solvents" PS4K and PS23K. (a) Storage (G') and loss (G'') moduli of the PS790K/PS4K blend and PS4K. Circles: PS790K/PS4K. Diamonds: PS4K. The master curves are constructed by the time–temperature superposition principle at the reference temperature T_{ref} = 130 °C. (b) Data for the PS790K/PS23K blend and the neat PS23K at T_{ref} = 130 °C. (c) Data for the PS130K/PS12K blend and the neat PS12K at T_{ref} = 120 °C. (d) Data for the PS790K/Pα MS11K blend and the neat Pα MS11K at T_{ref} = 200 °C.
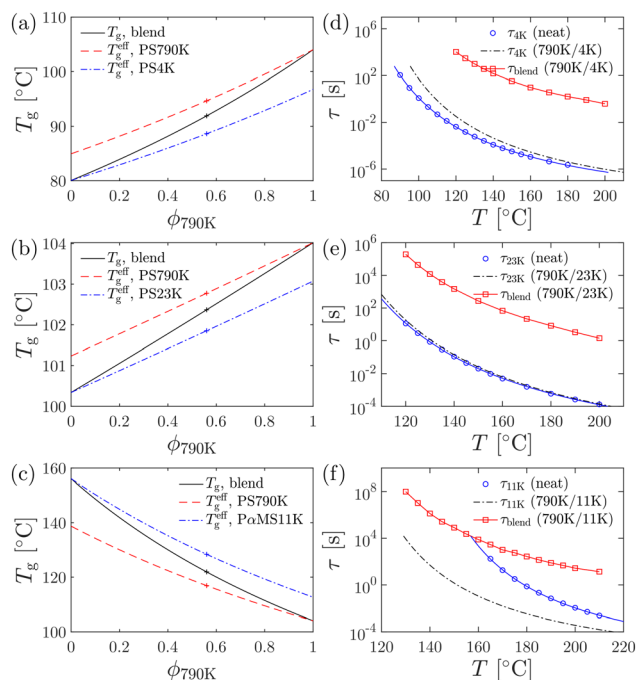
Fig. 7 (a)–(c) Composition dependence of the blend glass transition temperature T_g and the effective component glass transition temperature T_g^{eff}, which are calculated according to the Fox equation and the Lodge–McLeish model, respectively. Solid lines: T_g of the blend. Dashed lines: T_g^{eff} of the long chain. Dash-dotted lines: T_g^{eff} of the short chain. The crosses indicate the glass transition temperatures at the experimental compositions. (d)–(f) Temperature dependence of relaxation time. Circles: terminal relaxation time of the neat short chain melt. Dash-dotted lines: terminal relaxation time of the short chain in the blend. Squares: terminal relaxation time of the blend (long chain).

The majority of these systems have been shown to go through demixing (concentration fluctuations) under either extensional[60,65,72] or shear deformation.[55,56,59,61,62,115,116] In particular, light-scattering experiments have revealed deformation-induced demixing of the PS/DOP solutions in both shear and extensional flows.[60,115] Additionally, what the polystyrene/oligostyrene blends and the aforementioned polymer solutions have in common is that the solvent has a lower glass transition temperature than the long-chain solute. Deformation-induced demixing is thus expected to elevate the T_g of the long chain, giving rise to enhanced local friction. Conceptually, the coupling between stress and diffusion[69,100,117] exists, regardless of the mode of deformation.[69,99,101,102,118] As a result, deformation-induced demixing should be prevalent in multicomponent polymeric systems, including polymer blends and solutions.

4 Summary

In summary, small-angle neutron scattering experiments demonstrate that deformation-induced demixing occurs in polystyrene–oligostyrene blends both during continuous stretching and after a step extension. This process is driven

by the coupling between stress and diffusion, and takes place on time scales longer than the characteristic relaxation time of the short chain. Demixing changes the effective glass transition temperature and thereby the local friction of the long chain. Two consequences associated with the friction change are discussed, namely, the molecular weight effect and temperature effect. A survey of the literature further suggests that deformation-induced demixing should be present in the majority of the polymer blends and solutions recently investigated by extensional rheology. These findings call attention to the influence of deformation-induced demixing on polymer segmental friction, and offer important clues for understanding the nonuniversal behavior of polymers in extensional flow. It is worth noting that the present study by no means suggests that deformation-induced demixing is the only mechanism for changing segmental friction. Indeed, an apparent reduction in segmental friction has been observed by Matsumiya et al. in unentangled polymer melts,[31] where demixing is evidently absent. More studies are clearly desired to fully resolve the variation of local friction of polymers in the nonlinear rheological regime.

The presence of deformation-induced demixing poses significant theoretical challenges for the rheology of polymeric mixtures. For example, the spatial distribution of local friction and entanglement density in systems undergoing demixing is still an open question. The existing hydrodynamic theories[98–102] are formulated on the continuum level, and do not have any "feedback" mechanism to incorporate the effect of concentration fluctuations on segmental friction or entanglement density. Moreover, when clear phase boundaries are formed, the influence of surface tension[119,120] on the rheological response may also be considered.

Finally, we point out that the influence of concentration fluctuations on the segmental dynamics of miscible polymer blends in the equilibrium state has been well recognized and widely discussed in the literature.[113,121–124] In this context, the present work can be regarded as a conceptual extension of this effect to the nonequilibrium state, where the coupling between stress and diffusion drives large concentration fluctuations (demixing) in polymer blends and solutions with viscoelastic asymmetry. The large deformation-induced concentration fluctuations have profound influences on the polymer segmental friction, and pose a tremendous challenge to the theoretical modeling of multicomponent polymeric materials.

Author contributions

Y. Wang: conceptualization (lead); data curation (equal); investigation (equal); methodology (equal); formal analysis (equal); writing – original draft (lead); writing – review & editing (equal). S. Patil: data curation (equal); investigation (equal); methodology (equal); formal analysis (equal). C. Do: data curation (equal); writing – review & editing (equal). S. Cheng: data curation (equal); investigation (equal); methodology (equal); formal analysis (equal); writing – review & editing (equal).

Conflicts of interest

There are no conflicts to declare.

Appendices

Appendix A: Linear viscoelasticity

This section provides additional information about the linear viscoelastic properties of the polymer blends as well as the neat short-chain "solvents". As stated in the main text, small-amplitude oscillatory shear measurements were employed to evaluate the dynamic mechanical spectra of these samples, and the resulting master curves are shown in Fig. 6. In all cases, including the PS790K/PαMS11K blend, the time–temperature superposition principle works reasonably well, which is consistent with the miscible nature of these blends. It is also apparent from the linear viscoelastic spectra that in the PS/PS blends the short chains have lower glass transition temperatures than the blends, whereas the opposite scenario is encountered in the PS790K/PαMS11K blend.

Appendix B: Component dynamics in equilibrium

Analysis of the nonlinear rheological behavior of binary polymer blends requires an estimation of the characteristic relaxation times of both components in equilibrium. The terminal relaxation time of the long chain in the blends can be conveniently calculated from the low-frequency crossover (ω_c) of the storage and loss moduli in the linear viscoelastic spectra as $\tau = 1/\omega_c$. However, the determination of the short-chain relaxation time is often not straightforward, due to the lack of clear viscoelastic signatures of short chain motions. To gain insights into the component dynamics of the polymer blends, the Lodge–McLeish model[84] is employed.

The key concept in this model is the self-concentration ϕ_{self}, which describes the deviation of the local environment of a segment in a miscible polymer blend as a result of chain connectivity. The self-concentration can be estimated as[84]

$$\phi_{\text{self}} = \frac{C_\infty m_0}{k \rho_0 N_A l_K^3} = \frac{m_0}{C_\infty^2 k l^3 \rho_0 N_A}, \qquad (B.1)$$

where m_0 is the molecular weight of the repeating unit, ρ_0 is the polymer mass density, N_A is Avogadro's constant, k is the number of bonds per repeating unit, C_∞ is the characteristic ratio, l is the bond length, and $l_K = C_\infty l$ is the Kuhn segment length. As stated in the main text, the following glassy state densities (ρ_0) are used in our calculations: 1.05 g cm^{-3} for h-PS,[74] 1.065 g cm^{-3} for h-PαMS,[74] and 1.12 g cm^{-3} for d-PS.[75] The bond length is 1.54 Å. The characteristic ratio is set to $C_\infty = 9.5$ for PS[84] and $C_\infty = 10.5$ for PαMS.[125] These parameters yield self-concentrations of $\phi_{\text{self}} = 0.25$ for PS and 0.23 for PαMS.

For a miscible polymer blend consisting of two components A and B, the effective, "local" volume fraction of a segment is given by

$$\begin{aligned} \phi_{\text{eff,A}} &= \phi_{\text{self,A}} + \left(1 - \phi_{\text{self,A}}\right)\phi_A, \\ \phi_{\text{eff,B}} &= \phi_{\text{self,B}} + \left(1 - \phi_{\text{self,B}}\right)\phi_B, \end{aligned} \qquad (B.2)$$

where ϕ_A and ϕ_B respectively are the macroscopic volume fractions of A and B, with $\phi_A + \phi_B = 1$.

Using the Fox equation,[84,126,127] the effective glass transition temperature T_g^{eff} for each component can be calculated as

$$\begin{aligned} \frac{1}{T_{g,A}^{\text{eff}}(\phi_A)} &= \frac{\phi_{\text{eff,A}}(\phi_A)}{T_{g,A}} + \frac{1 - \phi_{\text{eff,A}}(\phi_A)}{T_{g,B}}, \\ \frac{1}{T_{g,B}^{\text{eff}}(\phi_B)} &= \frac{1 - \phi_{\text{eff,B}}(\phi_B)}{T_{g,A}} + \frac{\phi_{\text{eff,B}}(\phi_B)}{T_{g,B}}, \end{aligned} \qquad (B.3)$$

where $T_{g,A}$ and $T_{g,B}$ are the glass transition temperatures of the neat polymers A and B, respectively, and $\phi_{\text{eff,A}}$ and $\phi_{\text{eff,B}}$ are described by eqn (2). Fig. 7(a)–(c) show the dependence of the blend glass transition temperature T_g and the effective component glass transition temperature T_g^{eff} on the nominal volume fraction of the long chain (PS790K). By design, the effective glass transition temperature of the short chain is higher than that of the long chain in the PS790K/PαMS11K blend, whereas the situation is reversed in the other two blends.

To estimate the terminal relaxation time of the short, unentangled chain in the blend, we follow the approach of Pathak et al.,[85] and make the assumption that the terminal relaxation time τ is determined by the effective glass transition temperature T_g^{eff} and can be described by the Williams–Landel–Ferry (WLF) equation:[4]

$$\log_{10}\left[\frac{\tau(\phi)}{\tau_g}\right] = \frac{-C_1\left[T - T_g^{\text{eff}}(\phi)\right]}{T - T_g^{\text{eff}}(\phi) + C_2}, \qquad (B.4)$$

where the parameters τ_g, C_1, and C_2 are independent of the composition, and can be obtained from viscoelastic measurements of the neat polymer. The results of the calculations are shown in Fig. 7(d)–(f). Alternatively, the terminal relaxation times of the short chains can also be estimated by superimposing the transition region[4] of the short-chain sample with that of the corresponding blend. Our calculations show that while this method yields different values for the short-chain relaxation times, the conclusions of the current study are not affected—these estimates are only used to establish the relative time scale of long-chain deformation or relaxation with respect to the short-chain dynamics.

Acknowledgements

Notes and references

1 G. C. Berry and T. G. Fox, *Adv. Polym. Sci.*, 1968, **5**, 261–357.

2 W. W. Graessley, *Adv. Polym. Sci.*, 1974, **16**, 1–179.

3 P. G. de Gennes, *Scaling Concepts in Polymer Physics*, Cornell University Press, New York, 1979.

4 J. D. Ferry, *Viscoelastic Properties of Polymers*, John Wiley & Sons, New York, 1980.

5 M. Doi and S. F. Edwards, *The Theory of Polymer Dynamics*, Oxford University Press, Oxford, 1986.

6 R. B. Bird, R. C. Armstrong and O. Hassager, *Dynamics of Polymeric Liquids. Fluid Mechanics*, John Wiley & Sons, New York, 2nd edn, 1987, vol. 1.

7 R. B. Bird, C. F. Curtiss, R. C. Armstrong and O. Hassager, *Dynamics of Polymeric Liquids, Kinetic Theory*, John Wiley & Sons, New York, 2nd edn, 1987, vol. 2.

8 R. G. Larson, *Constitutive Equations for Polymer Melts and Solutions*, Butterworths Publishers, Stoneham, 1988.

9 H. Watanabe, *Prog. Polym. Sci.*, 1999, **24**, 1253–1403.

10 M. Rubinstein and R. H. Colby, *Polymer Physics*, Oxford University Press, New York, 2003.

11 W. W. Graessley, *Polymeric Liquids and Networks: Dynamics and Rheology*, Garland Science, New York, 2008.

12 M. Takahashi, T. Masuda, N. Bessho and K. Osaki, *J. Rheol.*, 1980, **24**, 517–520.

13 W. W. Graessley, *Adv. Polym. Sci.*, 1982, **47**, 67–117.

14 E. Menezes and W. Graessley, *J. Polym. Sci., Part B: Polym. Phys.*, 1982, **20**, 1817–1833.

15 K. Osaki, *Rheol. Acta*, 1993, **32**, 429–437.

16 K. Osaki, T. Inoue and T. Isomura, *J. Polym. Sci., Part B: Polym. Phys.*, 2000, **38**, 1917–1925.

17 S. Ravindranath and S.-Q. Wang, *J. Rheol.*, 2008, **52**, 681–695.

18 D. Auhl, J. Ramirez, A. E. Likhtman, P. Chambon and C. Fernyhough, *J. Rheol.*, 2008, **52**, 801–835.

19 P. E. Boukany, S.-Q. Wang and X. Wang, *J. Rheol.*, 2009, **53**, 617–629.

20 S. Costanzo, Q. Huang, G. Ianniruberto, G. Marrucci, O. Hassager and D. Vlassopoulos, *Macromolecules*, 2016, **49**, 3925–3935.

21 P. Bhattacharjee, J. Oberhauser, G. H. McKinley, L. Leal and T. Sridhar, *Macromolecules*, 2002, **35**, 10131–10148.

22 P. Bhattacharjee, D. A. Nguyen, G. H. McKinley and T. Sridhar, *J. Rheol.*, 2003, **47**, 269–290.

23 X. Ye, R. G. Larson, C. Pattamaprom and T. Sridhar, *J. Rheol.*, 2003, **47**, 443–468.

24 A. Bach, K. Almdal, H. K. Rasmussen and O. Hassager, *Macromolecules*, 2003, **36**, 5174–5179.

25 J. K. Nielsen, H. K. Rasmussen, O. Hassager and G. H. McKinley, *J. Rheol.*, 2006, **50**, 453–476.

26 Q. Huang, N. J. Alvarez, Y. Matsumiya, H. K. Rasmussen, H. Watanabe and O. Hassager, *ACS Macro Lett.*, 2013, **2**, 741–744.

27 Q. Huang, O. Mednova, H. K. Rasmussen, N. J. Alvarez, A. L. Skov, K. Almdal and O. Hassager, *Macromolecules*, 2013, **46**, 5026–5035.

28 T. Sridhar, M. Acharya, D. A. Nguyen and P. K. Bhattacharjee, *Macromolecules*, 2014, **47**, 379–386.

29 Q. Huang, L. Hengeller, N. J. Alvarez and O. Hassager, *Macromolecules*, 2015, **48**, 4158–4163.

30 Q. Huang and H. K. Rasmussen, *J. Rheol.*, 2016, **60**, 465–471.

31 Y. Matsumiya, H. Watanabe, Y. Masubuchi, Q. Huang and O. Hassager, *Macromolecules*, 2018, **51**, 9710–9729.

32 H. K. Rasmussen, S. L. Wingstrand and O. Hassager, *Rheol. Acta*, 2019, **58**, 333–340.

33 R. Yuan, J. Liu, Y. Wang and S.-Q. Wang, *Soft Matter*, 2020, **16**, 3705–3716.

34 G. Marrucci and G. Ianniruberto, *Macromolecules*, 2004, **37**, 3934–3942.

35 G. Ianniruberto, A. Brasiello and G. Marrucci, *et al.*, *Proc. 7th Annu. Eur. Rheol. Conf*, 2011, p. 61.

36 G. Ianniruberto, A. Brasiello and G. Marrucci, *Macromolecules*, 2012, **45**, 8058–8066.

37 G. Ianniruberto, *Macromolecules*, 2015, **48**, 6306–6312.

38 G. W. Park and G. Ianniruberto, *Macromolecules*, 2017, **50**, 4787–4796.

39 T. Yaoita, T. Isaki, Y. Masubuchi, H. Watanabe, G. Ianniruberto and G. Marrucci, *Macromolecules*, 2012, **45**, 2773–2782.

40 Y. Masubuchi, Y. Matsumiya and H. Watanabe, *Macromolecules*, 2014, **47**, 6768–6775.

41 G. Ianniruberto, A. Brasiello and G. Marrucci, *Macromolecules*, 2019, **52**, 4610–4616.

42 A. Silberberg and W. Kuhn, *Nature*, 1952, **170**, 450–451.

43 J. Eliassaf, A. Silberberg and A. Katchalsky, *Nature*, 1955, **176**, 1119.

44 A. Lodge, *Polymer*, 1961, **2**, 195–201.

45 A. Peterlin and D. Turner, *J. Polym. Sci., Part B: Polym. Lett.*, 1965, **3**, 517–520.

46 I. Steg and D. Katz, *J. Appl. Polym. Sci.*, 1965, **9**, 3177–3193.

47 Y. Go, S. Matsuzawa, Y. Kondo and K. Nakamura, *Kobunshi Kagaku*, 1967, **24**, 577.

48 F. Frank, A. Keller and M. Mackley, *Polymer*, 1971, **12**, 467–473.

49 C. Rangel-Nafaile, A. Metzner and K. Wissbrun, *Macromolecules*, 1984, **17**, 1187–1195.

50 J. D. Katsaros, M. F. Malone and H. H. Winter, *Polym. Bull.*, 1986, **16**, 83–88.

51 M. Tirrell, *Fluid Phase Equilib.*, 1986, **30**, 367–380.

52 M. G. Brereton, T. A. Vilgis and F. Boué, *Macromolecules*, 1989, **22**, 4051–4053.

53 J. Bastide, L. Leibler and J. Prost, *Macromolecules*, 1990, **23**, 1821–1825.

54 F. Boué, J. Bastide, M. Buzier, A. Lapp, J. Herz and T. Vilgis, *Colloid Polym. Sci.*, 1991, **269**, 195–216.

55 X.-L. Wu, D. Pine and P. Dixon, *Phys. Rev. Lett.*, 1991, **66**, 2408.

56 T. Hashimoto and T. Kume, *J. Phys. Soc. Jpn.*, 1992, **61**, 1839–1843.

57 I. Hindawi, J. Higgins and R. Weiss, *Polymer*, 1992, **33**, 2522–2529.

58 R. Larson, *Rheol. Acta*, 1992, **31**, 497–520.

59 J. J. Magda, C. S. Lee, S. J. Muller and R. G. Larson, *Macromolecules*, 1993, **26**, 1696–1706.

60 J. W. van Egmond and G. G. Fuller, *Macromolecules*, 1993, **26**, 7182–7188.

61 F. Boué and P. Lindner, *Europhys. Lett.*, 1994, **25**, 421.

62 E. Moses, T. Kume and T. Hashimoto, *Phys. Rev. Lett.*, 1994, **72**, 2037–2040.

63 D. Wirtz, *Phys. Rev. E: Stat., Nonlinear, Soft Matter Phys.*, 1994, **50**, R1755.

64 A. Ramzi, F. Zielinski, J. Bastide and F. Boué, *Macromolecules*, 1995, **28**, 3570–3587.

65 C. Hayes, L. Bokobza, F. Boué, E. Mendes and L. Monnerie, *Macromolecules*, 1996, **29**, 5036–5041.

66 E. Mendes, R. Oeser, C. Hayes, F. Boué and J. Bastide, *Macromolecules*, 1996, **29**, 5574–5584.

67 K. Migler, C.-H. Liu and D. Pine, *Macromolecules*, 1996, **29**, 1422–1432.

68 H. Murase, T. Kume, T. Hashimoto, Y. Ohta and T. Mizukami, *Macromol. Symp.*, 1996, 159–182.

69 A. Onuki, *J. Phys.: Condens. Matter*, 1997, **9**, 6119.

70 I. Morfin, P. Lindner and F. Boué, *Macromolecules*, 1999, **32**, 7208–7223.

71 N. Jouault, F. Dalmas, S. Said, E. Di Cola, R. Schweins, J. Jestin and F. Boué, *Phys. Rev. E: Stat., Nonlinear, Soft Matter Phys.*, 2010, **82**, 031801.

72 Y. Wang, W. Wang, K. Hong and Y. Liu, *Macromolecules*, 2021, **54**, 3531–3542.

73 S. Liu, L. Peng, S. Xiang, H. Chen, Y. Huang, X. Huang and Q. Huang, *ACS Macro Lett.*, 2024, **13**, 138–143.

74 D. W. Van Krevelen and K. Te Nijenhuis, *Properties of polymers: their correlation with chemical structure; their numerical estimation and prediction from additive group contributions*, Elsevier, Amsterdam, 4th edn, 2009.

75 W. Wallace, N. Beck Tan, W. Wu and S. Satija, *J. Chem. Phys.*, 1998, **108**, 3798–3804.

76 M. L. Sentmanat, *Rheol. Acta*, 2004, **43**, 657–669.

77 Z. Wang, C. N. Lam, W.-R. Chen, W. Wang, J. Liu, Y. Liu, L. Porcar, C. B. Stanley, Z. Zhao, K. Hong and Y. Wang, *Phys. Rev. X*, 2017, **7**, 031003.

78 C. N. Lam, W.-S. Xu, W.-R. Chen, Z. Wang, C. B. Stanley, J.-M. Y. Carrillo, D. Uhrig, W. Wang, K. Hong, Y. Liu, L. Porcar, C. Do, G. S. Smith, B. G. Sumpter and Y. Wang, *Phys. Rev. Lett.*, 2018, **121**, 117801.

79 Y. Wang, W. Wang, K. Hong, C. Do and W.-R. Chen, *Polymer*, 2020, **204**, 122698.

80 R. Sun, M. Melton, N. Safaie, R. C. Ferrier Jr, S. Cheng, Y. Liu, X. Zuo and Y. Wang, *Phys. Rev. Lett.*, 2021, **126**, 117801.

81 Y. Wang, P. Boukany, S.-Q. Wang and X. Wang, *Phys. Rev. Lett.*, 2007, **99**, 237801.

82 P. Santangelo and C. Roland, *Macromolecules*, 1998, **31**, 4581–4585.

83 Y. Ding, A. Kisliuk and A. Sokolov, *Macromolecules*, 2004, **37**, 161–166.

84 T. P. Lodge and T. C. McLeish, *Macromolecules*, 2000, **33**, 5278–5284.

85 J. A. Pathak, S. K. Kumar and R. H. Colby, *Macromolecules*, 2004, **37**, 6994–7000.

86 J. K. Zhao, C. Y. Gao and D. Liu, *J. Appl. Cryst.*, 2010, **43**, 1068–1077.

87 W. T. Heller, M. Cuneo, L. Debeer-Schmitt, C. Do, L. He, L. Heroux, K. Littrell, S. V. Pingali, S. Qian, C. Stanley, V. S. Urban, B. Wu, W. Bras and IUCr, *J. Appl. Crystallogr.*, 2018, **51**, 242–248.

88 O. Arnold, J.-C. Bilheux, J. Borreguero, A. Buts, S. I. Campbell, L. Chapon, M. Doucet, N. Draper, R. F. Leal and M. Gigg, *et al.*, *Nucl. Instrum. Methods Phys. Res., Sect. A*, 2014, **764**, 156–166.

89 W. T. Heller, J. Hetrick, J. Bilheux, J. M. B. Calvo, W.-R. Chen, L. DeBeer-Schmitt, C. Do, M. Doucet, M. R. Fitzsimmons, W. F. Godoy, G. E. Granroth, S. Hahn, L. He, F. Islam, J. Lin, K. C. Littrell, M. McDonnell, J. McGaha, P. F. Peterson, S. V. Pingali, S. Qian, A. T. Savici, Y. Shang, C. B. Stanley, V. S. Urban, R. E. Whitfield, C. Zhang, W. Zhou, J. J. Billings, M. J. Cuneo, R. M. F. Leal, T. Wang and B. Wu, *SoftwareX*, 2022, **19**, 101101.

90 P. G. de Gennes, *Scaling Concepts in Polymer Physics*, Cornell University Press, New York, 1979.

91 J. S. Higgins and H. Benoît, *Polymers and Neutron Scattering*, Clarendon Press, Oxford, 1994.

92 J. Cotton, D. Decker, H. Benoit, B. Farnoux, J. Higgins, G. Jannink, R. Ober, C. D. Picot and J. Des Cloizeaux, *Macromolecules*, 1974, **7**, 863–872.

93 S. Saeki, J. Cowie and I. McEwen, *Polymer*, 1983, **24**, 60–64.

94 J.-M. Widmaier and G. Mignard, *Eur. Polym. J.*, 1987, **23**, 989–992.

95 L. Lanzavecchia and E. Pedemonte, *Thermochim. Acta*, 1988, **137**, 123–128.

96 A. Rameau, Y. Gallot, P. Marie and B. Farnoux, *Polymer*, 1989, **30**, 386–392.

97 C. N. Lam, L. He, C. Do, W.-R. Chen, W. Wang, K. Hong and Y. Wang, *J. Appl. Crystallogr.*, 2023, **56**, 1168–1179.

98 A. Onuki, *Phys. Rev. Lett.*, 1989, **62**, 2472.

99 E. Helfand and G. H. Fredrickson, *Phys. Rev. Lett.*, 1989, **62**, 2468.

100 S. T. Milner, *Phys. Rev. Lett.*, 1991, **66**, 1477.

101 H. Ji and E. Helfand, *Macromolecules*, 1995, **28**, 3869–3880.

102 M. Cromer, M. C. Villet, G. H. Fredrickson, L. G. Leal, R. Stepanyan and M. J. H. Bulters, *J. Rheol.*, 2013, **57**, 1211–1235.

103 J. J. Kirkensgaard, L. Hengeller, A. Dorokhin, Q. Huang, C. J. Garvey, K. Almdal, O. Hassager and K. Mortensen, *Phys. Rev. E*, 2016, **94**, 020502.

104 H. Tanaka, T. Araki, T. Koyama and Y. Nishikawa, *J. Phys.: Condens. Matter*, 2005, **17**, S3195.

105 H. Tanaka and T. Araki, *Chem. Eng. Sci.*, 2006, **61**, 2108–2141.

106 J. A. Kornfield, G. G. Fuller and D. S. Pearson, *Macromolecules*, 1989, **22**, 1334–1345.

107 M. Doi, D. Pearson, J. Kornfield and G. Fuller, *Macromolecules*, 1989, **22**, 1488–1490.

108 M. Doi and H. Watanabe, *Macromolecules*, 1991, **24**, 740–744.

109 J. Cao and A. E. Likhtman, *Phys. Rev. Lett.*, 2010, **104**, 207801.

110 R. H. Colby, *Polymer*, 1989, **30**, 1275–1278.

111 X. Yang, S.-Q. Wang and H. Ishida, *Macromolecules*, 1999, **32**, 2638–2645.

112 X. Yang, A. Halasa, W.-L. Hsu and S.-Q. Wang, *Macromolecules*, 2001, **34**, 8532–8540.

113 S. K. Kumar, R. H. Colby, S. H. Anastasiadis and G. Fytas, *J. Chem. Phys.*, 1996, **105**, 3777–3788.

114 S. L. Wingstrand, N. J. Alvarez, Q. Huang and O. Hassager, *Phys. Rev. Lett.*, 2015, **115**, 078302.

115 J. W. van Egmond, D. E. Werner and G. G. Fuller, *J. Chem. Phys.*, 1992, **96**, 7742–7757.

116 A. Nakatani, J. Douglas, Y.-B. Ban and C. Han, *J. Chem. Phys.*, 1994, **100**, 3224–3232.

117 M. Doi and A. Onuki, *J. Phys. II*, 1992, **2**, 1631–1656.

118 M. Cromer, G. H. Fredrickson and L. Gary Leal, *J. Rheol.*, 2017, **61**, 711–730.

119 D. Graebling, R. Muller and J. Palierne, *Macromolecules*, 1993, **26**, 320–329.

120 W. Yu, W. Zhou and C. Zhou, *Polymer*, 2010, **51**, 2091–2098.

121 S. Kamath, R. H. Colby, S. K. Kumar, K. Karatasos, G. Floudas, G. Fytas and J. E. Roovers, *J. Chem. Phys.*, 1999, **111**, 6121–6128.

122 S. Salaniwal, R. Kant, R. H. Colby and S. K. Kumar, *Macromolecules*, 2002, **35**, 9211–9218.

123 R. Kant, S. K. Kumar and R. H. Colby, *Macromolecules*, 2003, **36**, 10087–10094.

124 S. K. Kumar, S. Shenogin and R. H. Colby, *Macromolecules*, 2007, **40**, 5759–5766.

125 M. Kurata and Y. Tsunashima, in *Viscosit-ymolecular weight relationships and unperturbed dimensions of linear chain molecules*, ed. J. Brandrup, E. H. Immergut, E. A. Grulke, A. Abe and D. R. Bloch, John Wiley & Sons, New York, 1999.

126 G. Fox, *Bull. Am. Phys. Soc.*, 1956, **1**, 123.

127 H. A. Schneider and E. A. Di Marzio, *Polymer*, 1992, **33**, 3453–3461.